Classification of fold/hom and fold/Hopf spike-adding phenomena

Roberto Barrio,[1, a)] Santiago Ibáñez,[2, b)] Lucía Pérez,[2, c)] and Sergio Serrano[1, d)]
[1)] *Departamento de Matemática Aplicada and IUMA. Computational Dynamics group. University of Zaragoza. E-50009. Spain.*
[2)] *Departamento de Matemáticas. University of Oviedo. E-33007 Oviedo. Spain.*

(Dated: 25 June 2021)

Hindmarsh-Rose neural model is widely accepted as an important prototype for fold/hom and fold/Hopf burstings. In this paper we are interested in the mechanisms for the production of extra spikes in a burst, and we show the whole parametric panorama in an unified way. In the fold/hom case two types are distinguished, the continuous one, where the bursting periodic orbit goes through bifurcations, but persists along the whole process, and the discontinuous one, where the transition is abrupt and happens after a sequence of chaotic events. In the former case we speak about canard-induced spike-adding and, in the second one, about chaos-induced. For fold/Hopf bursting, a single (and continuous) mechanism is distinguished. Separately, all these mechanisms are presented, to some extent, in the literature. However, our full perspective allows us to construct a spike-adding map and, more significantly, to understand the dynamics exhibited when borders are crossed, that is, transitions between types of processes, a crucial point not previously studied.

Keywords: neuron models, fold/hom bursting, fold/Hopf bursting, spike-adding mechanisms
AMS codes: 37B10, 65P20, 92B20

Among the elements that allow communication between neurons, spikes or action potentials are major pieces. Spike trains (bursts) allow the brain to build a language for the transmission of information since they are signals with a higher probability of being picked up by neighbouring neurons than an isolated spike.[1] Moreover, the number and the temporal pattern of spikes provide a system for encoding messages. Facing this context, understanding how spikes can be gained (or lost) becomes a central question. This is the goal of this work, taking the Hindmarsh-Rose equations as a paradigm for certain classes of bursting, we analyse three different types of spike-adding processes. Although most of the involved dynamics and bifurcations are well known, we will be able to discover some novel characteristics. Our classification of the different spike-adding mechanisms determines maps in the parameter space that are shown to help in the global analysis of the system. But, as maps are useless if frontiers are unclear, in this work we deal with the dynamics that characterize the transitions from one to another type of spike-adding. Moreover, some common elements necessary in our discussion are also present in neural and other problems (mechanics, chemistry, ...), such as the existence in numerical and experimental studies of comb-shaped chaotic regions and the spike-adding phenomenon[2–5], so this work can help in the exploration of these systems. Challenges in neuroscience and, in particular, the problems that still remain to be solved in deciphering the language of neurons are impressive. Undoubtedly, the classification of the different mechanisms involved in the genesis of extra action potentials is an essential element of that big task.

[a)] Electronic mail: rbarrio@unizar.es
[b)] Electronic mail: mesa@uniovi.es
[c)] Electronic mail: perezplucia@uniovi.es
[d)] Electronic mail: sserrano@unizar.es

I. INTRODUCTION

Bursting is one of the most relevant phenomena that can be observed in a neuron. Roughly speaking, bursting is characterized by the appearance of sequences of spikes, corresponding to fast discharges, alternating with periods of quiescence. Moreover, when dealing with a bursting neuron, one of the major challenges is to understand how spikes are added to a given train of signals.

This paper studies the spike-adding mechanisms exhibited in the Hindmarsh-Rose[6] neuron model, a well known example and prototype of fold/hom (or square-wave) and fold/Hopf bursting[7,8]. It is able to reproduce the most significant behaviors: quiescence, spiking and also bursting, either regular or irregular (chaotic). Literature concerning this model is extensive and, only in relation to our interests, we can quote Refs. 2, 9–21.

The Hindmarsh-Rose (HR) model is described by the following set of equations:

$$\begin{cases} \dot{x} = y - ax^3 + bx^2 - z + I, \\ \dot{y} = c - dx^2 - y, \\ \dot{z} = \varepsilon[s(x - x_0) - z]. \end{cases} \tag{1}$$

Variable x represents the membrane potential, whereas y and z correspond to ionic currents. We consider a typical choice of parameters with $a = 1$, $c = 1$, $d = 5$ and $s = 4$, discussing the spike-adding processes for different choices of the other b, I and ε.[21] We assume that ε is a small parameter in the model, giving rise to a fast-slow system with two fast (x and y), and one slow (z) variables.

When $\varepsilon = 0$ in model (1), we obtain a reduced system which is usually called the fast subsystem. Note that the fast subsystem is a family of planar vector fields where z is an additional parameter. Fixing b and I (still with $\varepsilon = 0$), we obtain a bifurcation diagram with respect to z that is illustrated in Fig. 1. There is a curve formed by equilibria which is named the slow manifold ($\mathscr{M}_{slow}$) and a surface containing limit cy-

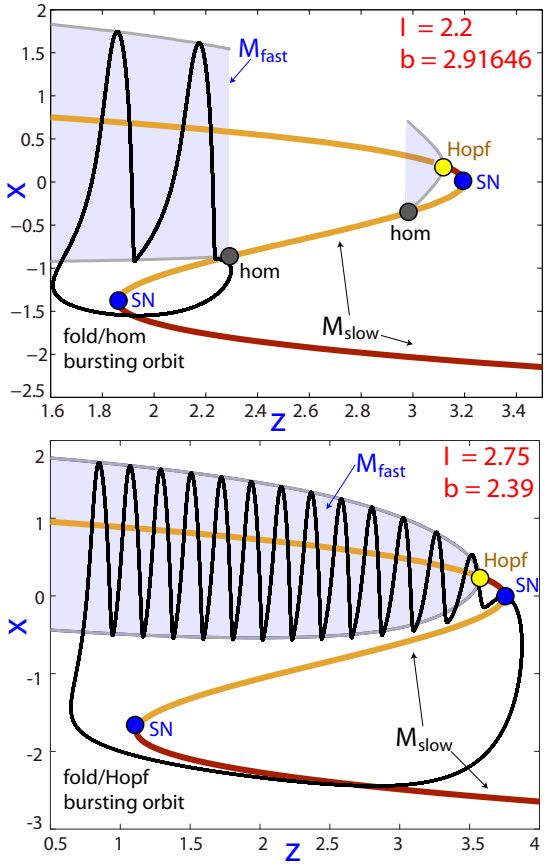

FIG. 1. 2D projection of fold/hom (top) and fold/Hopf (bottom) bursting orbits ($\varepsilon = 0.01$) superimposed (in black) over the classical slow-fast decomposition ($\varepsilon = 0$) of the HR model (1) formed by the 1D slow manifold of stable (dark red) and unstable (orange) equilibria ($\mathscr{M}_{slow}$) and the 2D fast (spiking) manifold ($\mathscr{M}_{fast}$) of limit cycles of the fast subsystem of the model (in gray). `SN` stands for saddle-node bifurcations of equilibria, `Hopf` denotes the Hopf bifurcation points and `hom` the homoclinic bifurcation points.

cles which is said the fast manifold ($\mathscr{M}_{fast}$). Recall that, in a general setting, slow-fast decompositions were first described in Ref. 7. For $I = 2.2$, $b = 2.91646$ (top) and for $I = 2.75$ and $b = 2.39$ (bottom), the slow manifold is shown in dark red (resp. orange) for stable (resp. unstable) equilibria and the fast manifold is shown in gray. Intuitively, one can understand how burst patterns emerge. Fig. 1 also shows stable periodic orbits of the full system (black) superimposed to the bifurcation diagram of the fast subsystem. The slow dynamics in the complete model is such that $\dot{z} < 0$ when fast variables are moving close to the lower branch of $\mathscr{M}_{slow}$, whereas $\dot{z} > 0$ when they are close to $\mathscr{M}_{fast}$.

Indeed, as singular perturbation theory and Fenichel's theorems explain[22], orbits (for small enough ε) follow both manifolds on some parts of their trajectory. Following the terminology in Ref. 8, in the first case (top panel), the bursting orbit is said to be of fold/homoclinic type, because the termination of the fast subregime is due to the existence of a homoclinic bifurcation in the phase space of the fast subsystem. In the second case (bottom panel), the bursting orbit is said to be of fold/Hopf type because the amplitude of oscillations during the bursting is decreasing as the limit cycles of the reduced model approach the Hopf bifurcation.

As already mentioned, the main goal of this paper is to explain the processes (spike-adding) that lead a bursting orbit to change its number of spikes per period. More precisely, we provide a classification of the different types of spike-adding processes in fold/hom and fold/Hopf bursters. From Terman[23], in the general context of fold/hom bursting, two spike-adding mechanisms are considered. On the one hand, there can arise extra excursions around the fast manifold which are generated through a discontinuous process linked to a chaotic phenomenon. On the other, there also can happen that extra excursions are created through a continuous process linked to orbits that transit through phase space following the unstable branch of the slow manifold. We will refer to the first scenario as chaos-induced spike-adding, and the second one as canard-induced spike-adding. Both cases have been recently studied in the literature[9,11,17,19,24]. Note that analytical results have only been obtained very recently on simpler models, such as the in-depth theoretical study on the spike-adding canard transition given by P. Carter in Ref. 25, where the Morris-Lecar model[26] is considered (see also Ref. 27 where a transition from 1 to 2 spikes via canard orbits is thoroughly analysed in a different fast-slow system based on the FitzHugh-Nagumo equations). These two interesting papers are the first analytical studies regarding the complete creation of canard orbits in neural models and open an exciting research line. However, it should be noted that the whole scenario is beyond the current analytical techniques.

The spike-adding mechanism in the case of fold/Hopf bursting is completely different and is related to the distance between saddle-node (left SN bifurcation point of Fig. 1(bottom)) and Hopf bifurcation points in the fast subsystem (see Fig. 1). Namely, the number of spikes depends on the length of the oscillation tube which is accessible for orbits after they jump to the fast manifold from the slow manifold. It also depends on the characteristic rotation speed at the Hopf bifurcation point. We will refer to this mechanism for spike-adding as Hopf-induced. Discussions in the literature about the spike-adding mechanism involved in the fold/Hopf bursters are not so common as those about fold/hom scenarios. Of course, in all cases, the number of spikes also increases as ε decreases, but this is not our interest, so we will consider fixed small values of ε.

We will see how the Hindmarsh-Rose model exhibits the three spike-adding mechanisms that we have just described. As said, all have already been considered, to a greater or a lesser extent, in the literature. However, in this paper the treatment is unified, which allows to understand the differences between them. Besides, we pay special attention to the transition dynamics between scenarios, a problem not well studied in literature. Bearing in mind that different spike-adding processes are feasible in a model (HR model in our case), the question is: where and why are they produced?

The frontier between the two spike-adding mechanisms linked to fold/hom bursters will be shown to be sharp. Namely, it will be marked by homoclinic surfaces in the

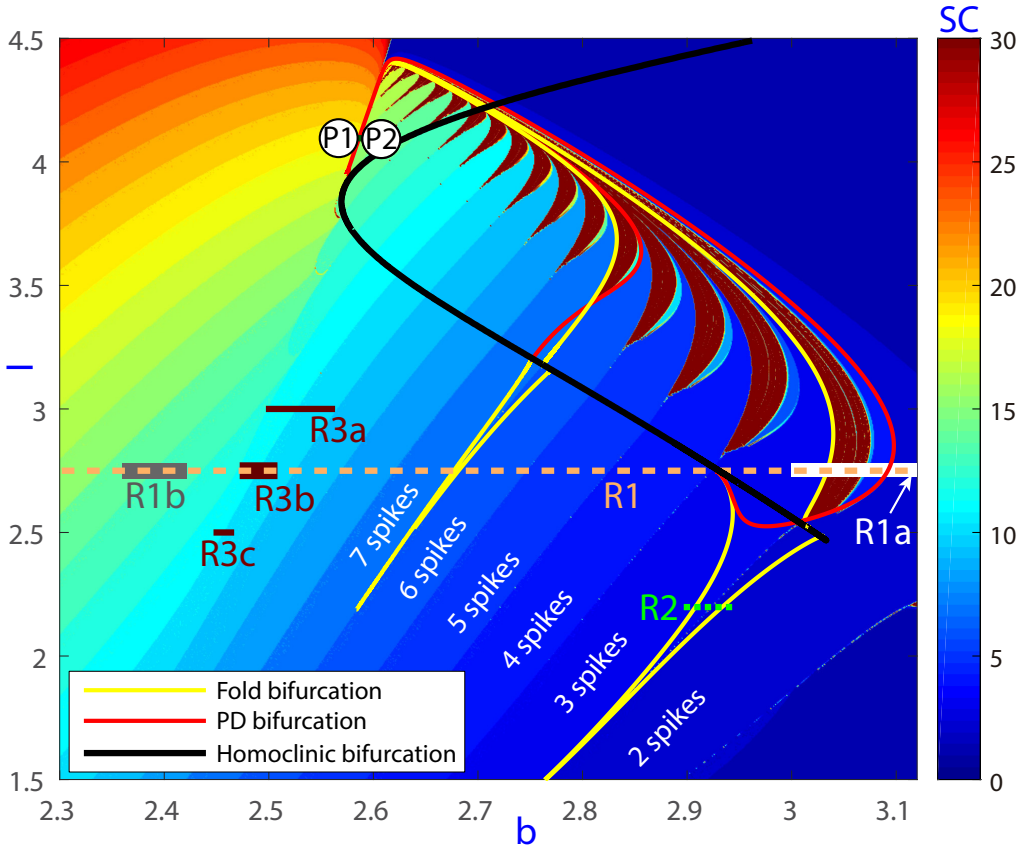

FIG. 2. Biparametric spike-counting bifurcation diagram for $\varepsilon = 0.01$. Different segments are selected to illustrate (on later figures) three different spike-adding processes: chaos-induced discontinuous spike-adding, canard-induced continuous spike-adding and Hopf-induced continuous spike-adding. Along the long segment $R1$ all of them appear; a discontinuous chaos-induced transition from 2 to 3 spikes along segment $R1a$; a continuous Hopf-induced transition from 13 to 14 spikes along segment $R1b$; and continuous canard-induced along segment $R2$ showing a transition from 2 to 3 spikes between fold/hom bursters. Transitions from $P1$ to $P2$ and along the segments $R3a$, $R3b$ and $R3c$ will be described in Section III to explain how dynamics evolve to change from one scenario to another.

three-parameter bifurcation diagram.[10] Nevertheless, the separation between Hopf-induced processes and either chaos-induced or canard-induced will appear fuzzy. Coming from the region of chaos-induced spike-adding, a fan of bifurcations must be crossed to enter into the region corresponding to Hopf-induced processes. These bifurcations arise from a codimension-two homoclinic bifurcation point. As we will recall later, in the case of a canard-induced spike-adding, the periodic orbit must undergo several periodic orbit bifurcations (bistability and hysteresis are present), among them two curves of fold bifurcations which disappear at cusp[28] bifurcation points. These codimension-two bifurcation points will play the role of boundary stones separating the canard domains from the Hopf ones. In other words, continuous spike-adding can be canard-induced or Hopf-induced. The first case happens when the continuation of the periodic orbit includes paths of unstable regime. When this course is not realizable because no bifurcation is accessible (the continuation curve is far from the cusp boundary stones), the gaining of extra spikes can be explained through a Hopf bifurcation process.

All the different types of spike-adding mechanisms are detailed in Section II, showing how they indeed arise in the Hindmarsh-Rose model. Transitions between these mechanisms will be described in Section III. Results are summarized and discussed in Section IV, where a theoretical classification parametric map is proposed. Conclusions are provided in Section V. Throughout this article, all the continuation analysis has been done using the well known software AUTO[29,30].

II. CLASSIFICATION OF SPIKE-ADDING PHENOMENA

In this section we describe the different spike-adding phenomena present in the HR model. On Fig. 2, regions with periodic attractors with a different number of spikes are represented in different colors (spike-counting technique). From dark blue, indicating spiking, towards red, the number of spikes of the periodic orbit grows. Dark red indicates that the maximum number of spikes considered in the method has been exceeded, meaning that in a large part of that region the dominant behavior is chaotic[2].

This figure shows a typical situation for small ε values (in this case $\varepsilon = 0.01$). There exist a finite collection of homoclinic bifurcation curves, the black curve represented in the

figure being one of them. All the others are so close that, if they were also depicted, they would overlap with each other (see details in Ref. 10). Located on such curves there also arise codimension-two homoclinic bifurcations from which many of the elements involved in the spike-adding processes emerge. As an illustration, Fig. 2 includes some codimension-one bifurcations of periodic orbits: fold (yellow) and period-doubling (red) curves. Below the homoclinic bifurcation curve, there are wedges corresponding to bistability regimes. These regions are bounded by a pair of fold bifurcations connecting through a cusp point. Above the homoclinic bifurcation curve, lobes of chaotic dynamics are formed containing pencils of period-doubling cascades. These lobes are limited by a fold bifurcation curve of periodic orbits and the first period-doubling cascade.

Segment $R1$ in Fig. 2 crosses regions of the biparametric plane showing the three types of spike-adding detected in the model. Along segment $R1a$ we will describe the chaos-induced discontinuous spike-adding (Subsection II A) and segment $R1b$ is selected to explain the Hopf-induced continuous spike-adding (Subsection II C). On the other hand, although canard-induced continuous spike-adding is also present along $R1$, segment $R2$ from Fig. 2 is selected for the purpose of illustration, because it provides a clearer display (Subsection II B).

A. Chaos-induced discontinuous spike-adding

The first type of spike-adding process that we are going to analyze is the chaos-induced discontinuous one. As we have already mentioned, this process occurs in the region above the homoclinic curve, this curve being a boundary of such region. In Fig. 3 we consider segment $R1a$ of Fig. 2 and we zoom in on the surrounding region with the spike counting technique. Below that picture, we show the interspike-interval bifurcation diagram (IBD) of this segment and the $\|\cdot\|_2$ norm of the periodic orbits obtained with continuation techniques (AUTO).

As we can see in the figure, to the right of the segment there is a bursting periodic attractor with 2 spikes. As b decreases, a typical scenario is present. Firstly, the periodic attractor undergoes a cascade of period-doubling bifurcations, until a chaotic attractor is generated. Within the chaotic region, narrow windows of regular behavior appear where new periodic orbits are generated. They will go through new bifurcations where they will become unstable joining to the chaotic invariant set. Finally, at a fold bifurcation, the chaotic invariant set stop being an attractor and two periodic orbits (one stable and one unstable) with 3 spikes are generated.

To show how the attractors evolve throughout this spike-adding phenomenon, in Fig. 4 we present the complete process. The central picture shows the bifurcation diagram obtained by continuation (AUTO) corresponding to the segment $R1a$ in Fig. 2. We have selected several values of b (marked in the central picture with small colored squares and numbers) for which we have plotted these orbits. For these values, the periodic orbits (solid line for stable, and dashed for unstable ones) and a chaotic attractor (for square $-6-$) are shown

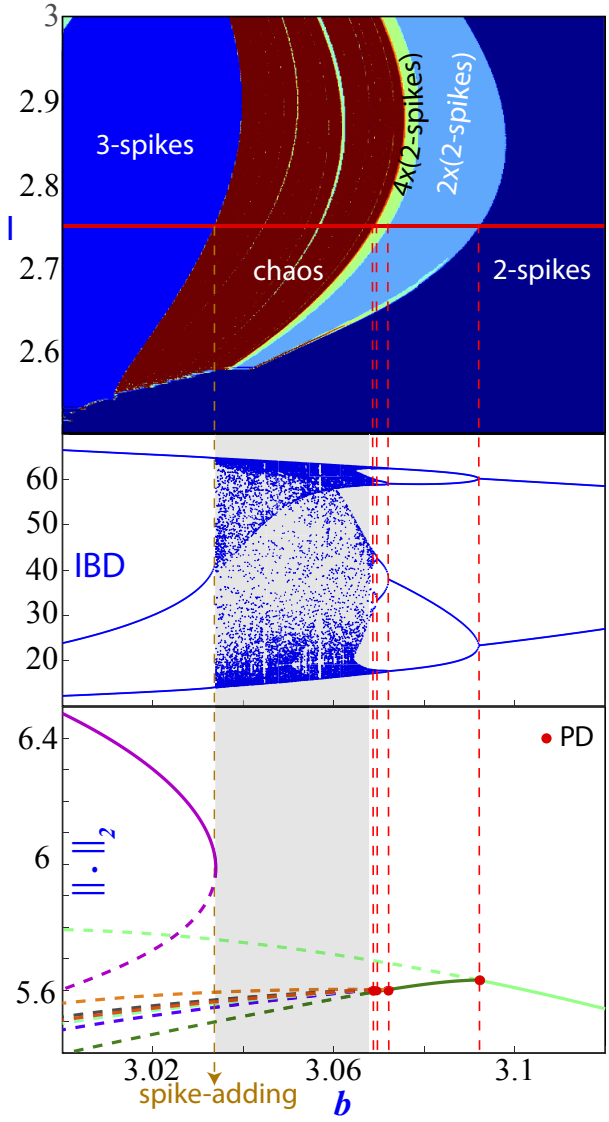

FIG. 3. Analysis of segment $R1a$ (in Fig. 2) with $\varepsilon = 0.01$, $I = 2.75$ and b as bifurcation parameter. Top: Biparametric bifurcation spike-counting diagram around the segment $R1a$. Dark red represents chaos, different colors represent periodic orbits with different bursting. Middle picture shows the IBD bifurcation diagram and the bottom one displays a continuation of the periodic orbits, with different solid (dashed) colors for different (un)stable orbits.

around the central picture. Orbit $-1-$ represents the basic periodic orbit of 2 spikes. After the first period-doubling bifurcation, the orbit $-1-$ becomes unstable and a stable periodic orbit ($-2-$) with two bursts with 2 spikes (2×2 orbit) is generated. A second period-doubling bifurcation repeats the former mechanism from 2×2 to 4×2 orbit ($-3-$). So, the same mechanism is developed again and again (to a 8×2 orbit $-4-$, 16×2 orbit $-5-$, and so on), a countably infinite number of times giving place to a typical period-doubling route to chaos that generates a chaotic attractor ($-6-$). After a fold bifurcation, the chaotic set becomes unstable and two periodic orbits ($-7-$) with 3 spikes are born (the spike-adding). One

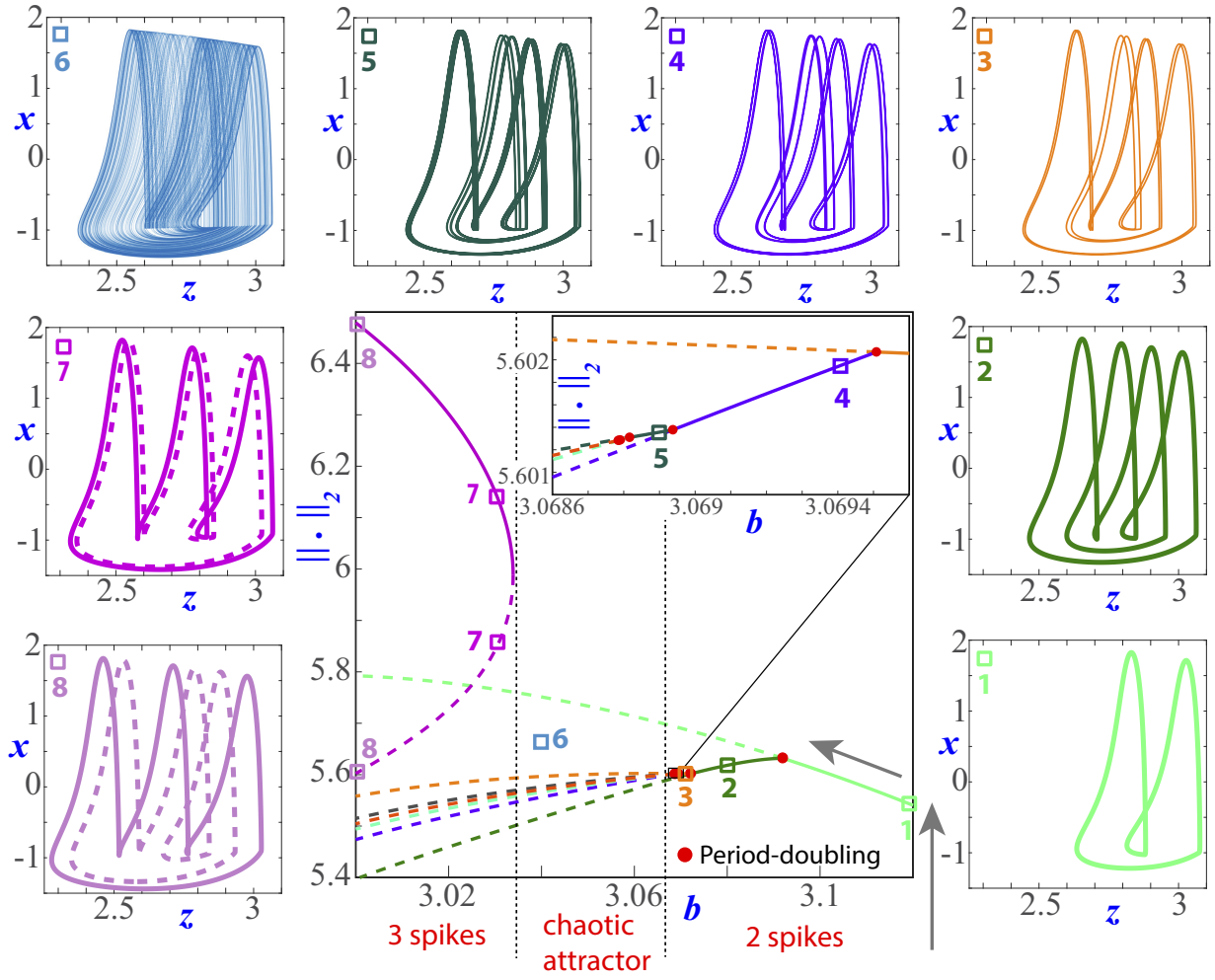

FIG. 4. Evolution of periodic orbits throughout the process of chaos-induced discontinuous spike-adding. Central picture shows the bifurcation diagram obtained by continuation corresponding to the segment $R1a$ in Fig. 2. The coloured squares mark the points in the diagram corresponding to the selected values. For these values, the periodic orbits (solid line for stable, and dashed for unstable ones) and a chaotic attractor (for square $-6-$) are shown around the central picture. Along the continuation of the bifurcation lines we observe periodic orbits with two spikes ($-1-$), later a period-doubling cascade ($-2-$ to $-5-$) originates a chaotic attractor ($-6-$) and, finally, after a fold bifurcation, two periodic orbits with three spikes appear ($-7-$ and $-8-$). In the upper right corner of the central picture, a magnification of the region where the first period-doubling cascade occurs is shown.

of them is stable, the other one unstable, both are indistinguishable at the fold bifurcation and they run along the outer edge of the chaotic set. When b moves away from the value at which the bifurcation occurs, both orbits are separated from each other.

It is worth paying attention to certain qualitative aspects that can be observed in the chaotic transition illustrated in Figure 4. As the attracting periodic orbits that arise through period-doublings build the chaotic attractor ($-6-$), spikes arrange visually in four groups inside phase space, although two of them, those placed in central positions, seem to compete to fill the same area. This process is typical in period-doubling cascades giving rise first to thin Feigenbaum chaotic attractors that later merge in thicker and larger ones via boundary crisis phenomena. When the chaotic attractor is fully created, we clearly see how the groups of spikes give rise to three, not to four, areas within the attractor, characterized by a denser flow. When the fold bifurcation occurs, the three-spiked stable periodic orbit takes the place of the chaotic attractor, flowing through the denser areas previously swept by the chaotic trajectory. The fold bifurcation marks the beginning of a periodic window: the chaotic attractor becomes an unstable saddle chaotic invariant set that embeds, among other unstable periodic orbits, the unstable orbit itself that is born at the fold bifurcation.

As already pointed out in Ref. 12, the process we have just described is known in the literature as Type I intermittency transition to chaos, as introduced in Refs. 31 and 32. In Ref. 12, authors explore a segment of parameters which cuts the whole sequence of chaotic lobes. The scenario here presented is common to each spike-adding. As b decreases, periodic orbits with n spikes go through a period-doubling cascade which

precedes the formation of a horseshoe. The dynamics enters into a chaotic window which disappears through a Type I intermittency transition. Chaotic transitions have been studied in Refs. 23 and 33. Working in a general framework, which includes the Hindmarsh-Rose model, Terman explains how the passage from n to $n+1$ spikes can be accompanied by the creation of horseshoes. In that sense, we understood that each passage through a chaotic lobe includes a Terman's transition.

B. Canard-induced continuous spike-adding

A full detailed picture of the continuous transition from 2 to 3 spikes between fold/hom bursters along the segment $R2$ (Fig. 2) is given in Fig. 5. In the central panel, the bifurcation curve obtained by continuation is displayed. Solid curve represents stable periodic orbits, while dashed curve indicates unstable periodic orbits. Squares with different colors over the curve mark different values of parameter b selected to show their corresponding periodic orbits (pictures around). These periodic orbits are plotted over the slow $\mathscr{M}_{slow}$ and fast $\mathscr{M}_{fast}$ manifolds of the limit case to explain the canard transition generating the new spike[11,13,17]. In the upper left corner of the central picture, all the selected orbits are represented together to see their relative position. Starting from the lower branch of the bifurcation curve, where the 2-spikes periodic orbit is stable, and decreasing the value of b, the curve reaches a fold bifurcation (marked with a square inside a circle). There, the periodic orbit becomes unstable and its length starts to increase as b decreases. This is the beginning of the canard transition: The increment in the length of the periodic orbit occurs as it extends following the piece of the slow manifold close to the unstable part of the manifold of equilibria between both fold bifurcations (see Fig. 1 top). Along the middle branch of the bifurcation curve, "headless" canards evolve up to a second fold bifurcation is reached. There, the orbit overcomes the right-fold of the equilibrium manifold in the fast subsystem and an additional turn around the tubular fast manifold arises; the canard orbit is said maximal and the canard "head" starts to be developed (second fold bifurcation marked with a square in a circle). This "head" moves to the left as b increases and the orbit recovers its stability after a period-doubling bifurcation (marked with a square inside a circle), when the orbit already has an extra spike. Therefore, the new spike has travelled from the neighbourhood of the right piece of $\mathscr{M}_{fast}$ to the neighbourhood of the left piece of $\mathscr{M}_{fast}$. This process that we have just described is the essential mechanism behind the continuous spike-adding for fold/hom bursters[11,13,17].

In the sense in which we have travelled the curve, the bifurcation where the orbit with three spikes regains its stability is actually a period-halving bifurcation. Keep in mind that in a small interval to the right of this bifurcation there are pencils of bifurcations very close each other, and so it is quite difficult to observe them and their effects. Just to show this, the doubled periodic orbit emerging at that point is also continued with AUTO and both bifurcation curves are displayed in Fig. 6 (light blue color lines). The curve for the double period orbit undergoes through a fold bifurcation where parameter b starts to increase until a second period-doubling is reached, and so on (note that the unstable orbit is connected with bifurcated orbits close to the fold on the right). This process only can be detected using continuation techniques because the stable region is very small and it has no real effects in the dynamics. However, once the phenomenon is detected, the orbits obtained can be carefully integrated to observe the chaotic behavior in that narrow parametric region (see red dots on the IBD on the top picture of Fig. 6).

This canard-induced spike-adding mechanism had already been discussed in the literature.[11,13,17,19] Some micro-chaos zones had already been detected and discussed in Ref. 12, but for segments very close to the homoclinic bifurcation curves, and not on the generic spike-adding process. Here we observe how small chaotic windows are detected far from the homoclinic skeleton. It follows that the fan of bifurcations of periodic orbits extends widely in parameter space. In fact, the chaotic window is associated with a cascade of period-doubling. The tangled bifurcation diagram formed by the codimension one bifurcations that arise from the codimension-two homoclinic bifurcation points has been discussed in Ref. 10, where it is also explained how the spike-adding mechanisms fit into the whole web.

C. Hopf-induced continuous spike-adding

The Hindmarsh-Rose model presents a variation of continuous spike-adding, where bistability and canards are not present. The spike-adding occurs without the periodic orbits losing their stability, but still increasing their length by adding an extra cycle to their turns around the fast manifold.

Unlike what happens in the fold/hom cases, in the process of Hopf-induced spike-adding, period-doubling and fold bifurcations do not appear. Neither is chaotic behavior observed, nor do canards emerge. The complete process is shown in Fig. 7, presenting again in the central panel the continuation bifurcation diagram of segment $R1b$ of Fig. 2. The coloured squares mark the points in the diagram corresponding to the selected values. For these values, the stable periodic orbits are shown over the slow $\mathscr{M}_{slow}$ and fast $\mathscr{M}_{fast}$ manifolds (see Fig. 1 for more details). As shown in Fig. 7, the process is straightforward. That is, what happens in this case is that, as b decreases, almost the entire orbit is moving toward smaller values of z. But the point of re-entry of the orbit around the fast manifold, after passing through the stable lower branch of the slow manifold, does not move. This means that more space is generated in the corner of the slow manifold where the upper saddle-node is located. Thus, there comes a time when there is room for a new spike in the orbit, which is occupied. As b continues to decrease, the displacement of most of the orbit continues, causing the amplitude of the new spike to increase. Along the continuation of the bifurcation line we observe how periodic orbits with thirteen spikes move to the left so that space is generated for the appearance of a new spike on the right side of the orbit giving rise to a burster with fourteen spikes instead of thirteen. If b continues to decrease sufficiently, this spike-adding process will be

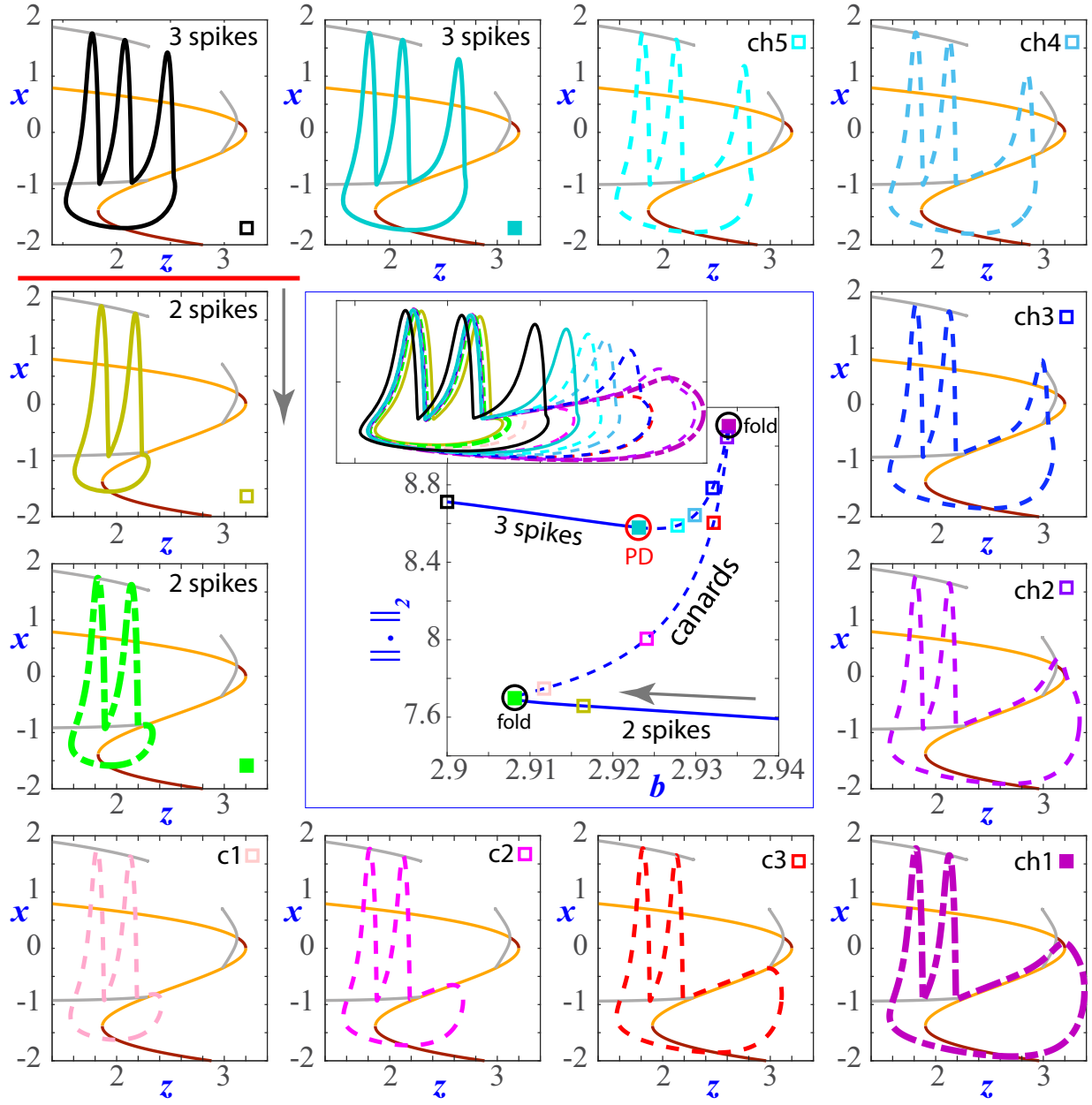

FIG. 5. Evolution of periodic orbits throughout the process of canard-induced continuous spike-adding. Central picture shows the bifurcation diagram obtained by continuation (AUTO) corresponding to the segment $R2$ in Fig. 2. The coloured squares mark the points in the diagram corresponding to the selected values. For these values, the periodic orbits (solid line for stable, and dashed for unstable ones) are shown over the slow and fast manifolds ($\mathscr{M}_{slow}$ and $\mathscr{M}_{fast}$, see Fig. 1 for more details). The grey arrow indicates the direction in the process of adding a new spike. In the upper left corner of the central picture, all the selected orbits are represented together to see their relative position. Along the continuation of the bifurcation line we observe periodic orbits with two spikes, later headless canards (orbits numbered with -c-), canards with head (-ch- orbits), and, finally, orbits with three spikes.

repeated in the same way.

As already mentioned in the introduction, any process of spike-adding where periodic orbits do not cross any bifurcation, just a smooth change allowing an extra spike, will be referred as Hopf-induced, even in the case where the fast dynamics does not correspond to a fold/Hopf bursting from the Izhikevich classification.

In the Appendix we explain theoretically, using a simple model, how the number of spikes depends on the distance between the two saddle-node bifurcation points of the slow manifold of equilibria $\mathscr{M}_{slow}$. In the case of a fold/Hopf burster, the number of spikes exhibited by an orbit is strongly linked to the size of the oscillation region in the phase space. The trajectory around the fast manifold is longer as greater is the width of that region in the direction of variable z and that width corresponds to the distance between the saddle-node bifurcation

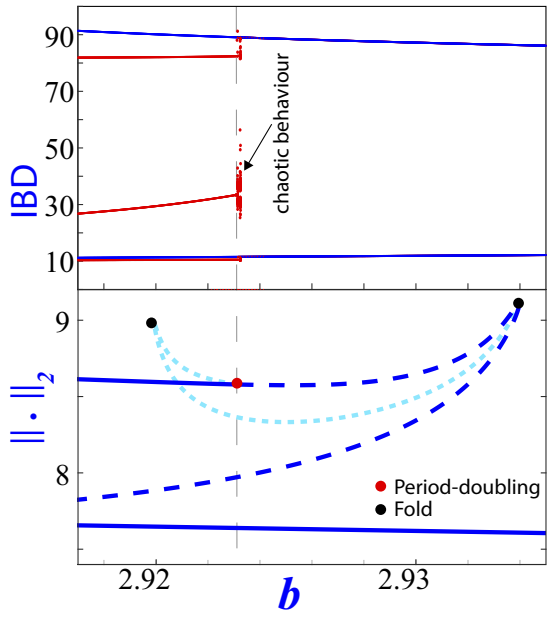

FIG. 6. IBD (top) and continuation diagram (bottom) of a magnification of segment $R2$. On the top picture, blue represents periodic orbits with two spikes while red line represents periodic orbits with three spikes and some bifurcated orbits from them coexisting with the two spikes periodic orbits. In the pointed thin region there exists chaotic behavior (dotted red points) originated via a very narrow period-doubling cascade.

points, at least for small values of ε . As b decreases, that distance increases. To be precise, observe how the lower saddle-node point moves to left as b decreases, but the upper one seems to remain fixed.

III. TRANSITION SPIKE-ADDING STATES

In the previous section we have identified three different spike-adding processes, namely, mechanisms induced by chaotic behaviors, canard explosions or Hopf bifurcations. Recall that the former is a discontinuous evolution, whereas the latter two are continuous transitions. Now we explain how the dynamics is transformed to change from one type to another.

We begin by discussing the transition between the two types of continuous spike-adding. In this case we cannot visually identify a sharp border marking the passage from one to the other. Fig. 8 shows the spike-adding process from bursting periodic orbits with 10 spikes to periodic orbits with 11 spikes along the three small segments $R3a$, $R3b$ and $R3c$ (see Fig. 2). Along the first segment, the process clearly corresponds to canard-induced continuous spike-adding. In the case of the third segment, however, the process clearly is Hopf-induced continuous spike-adding. It is evident that, between these two segments, a bifurcation has to occur that generates the change between both types of spike-adding. However, for this value of ε we are not able to detect it numerically as the continuation software stops the calculation of the fold bifurcations. We show an intermediate segment ($R3b$) where the passage through the canard is not so apparent.

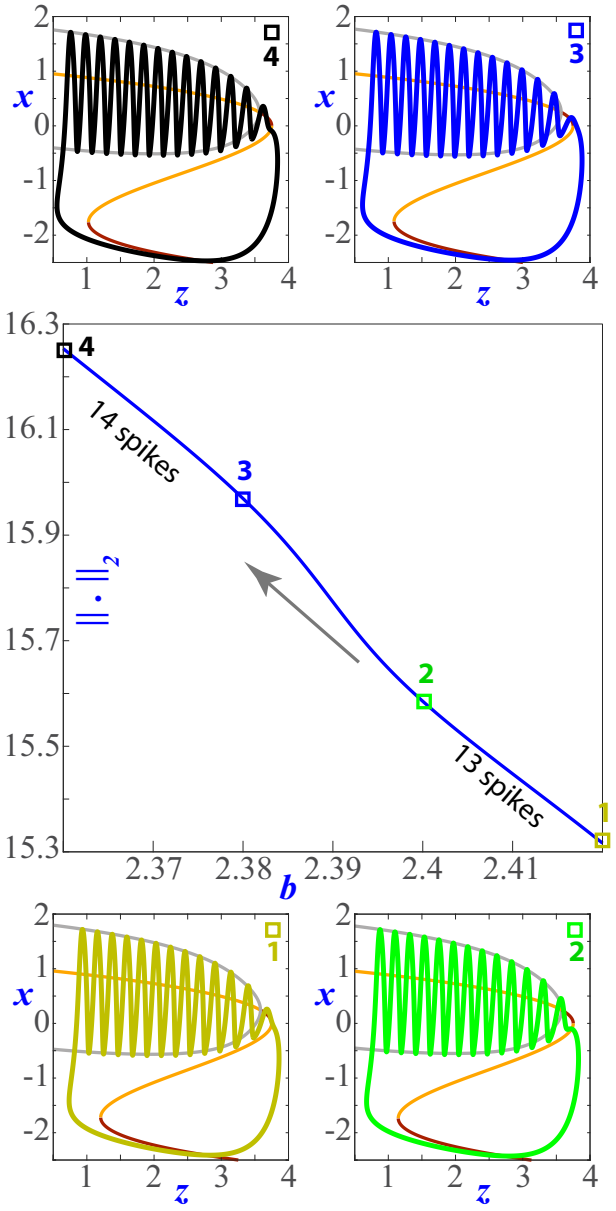

FIG. 7. Evolution of periodic orbits throughout the process of Hopf-induced continuous spike-adding. Central picture shows the bifurcation diagram obtained by continuation corresponding to the segment $R1b$ of Fig. 2. The coloured squares mark the points in the diagram corresponding to the selected values. The stable periodic orbits are shown over the slow $\mathscr{M}_{slow}$ and fast $\mathscr{M}_{fast}$ manifolds. The grey arrow indicates the direction in the process of adding a new spike. Along the continuation of the bifurcation line we observe how periodic orbits with thirteen spikes move to the left so that space is generated for the appearance of a new spike on the right side of the orbit. Finally, periodic orbits have fourteen spikes.

In order to illustrate more clearly the transition between these two types of spike-adding, we study one case for a

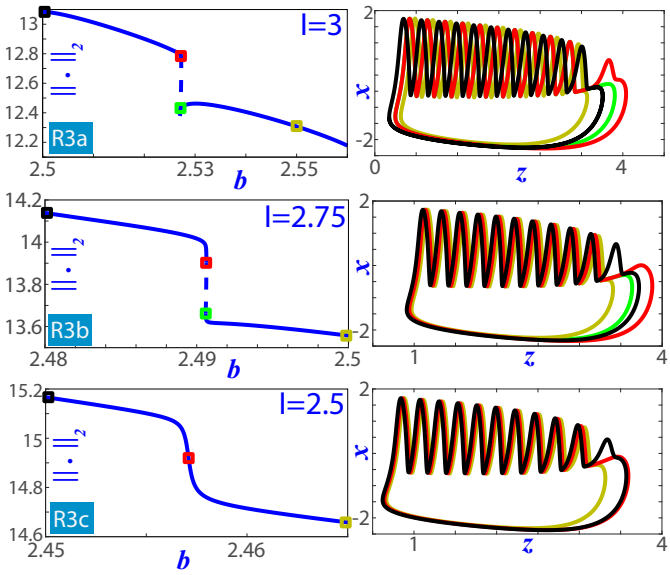

FIG. 8. Variations of the spike-adding processes along segments *R3a*, *R3b* and *R3c* (Fig. 2). Along segment *R3a* (top) the spike-adding is canard-induced, but along segment *R3c* (bottom) the bifurcation curve has been stretched and the spike-adding process is Hopf-induced.

higher value of the small parameter ($\varepsilon = 0.05$) to help in the visualization. For this ε value, the two fold bifurcations involved in the spike-adding from 2 to 3 spikes between fold/hom bursters that occur in the upper part of the region below the homoclinics can be fully continued numerically. Fold bifurcation curves are plotted in yellow in Fig. 9. They arise from codimension-two bifurcation points located on the homoclinic curves. Segments *A* and *B* cut both curves and, as it can be seen on the bottom pictures, the spike-adding process is canard-induced. If we compare the continuation bifurcation curves (left pictures) for both segments, we can observe how, as *I* decreases, the curve is stretched. As a consequence, the two fold bifurcation curves get closer to each other, until they reach a point (cusp bifurcation) where both coincide and disappear. Segment *C* goes through that point. This is the bifurcation point where canard-induced continuous spike-adding ends to give rise to Hopf-induced continuous spike-adding. Segments *D* and *E* cross this type of spike-adding, as can be seen on bottom pictures.

Once we understand how a cusp bifurcation of periodic orbits allows us to explain the passage from a canard-induced spike-adding towards a Hopf-induced type, we can conjecture that this is what happens for smaller values of ε and, in particular, in the case illustrated in Fig. 8, although the fold bifurcation curves involved are not easy to detect and to continue. It is important to remark here one main difference among both continuous spike-adding phenomena: in the canard-induced case the canard orbit in the process to obtain an extra spike makes a "go-and-come-back" excursion, whereas in the Hopf-induced case the orbit that is obtaining an extra spike grows but it does not come back. This is clearly seen in Figures 8

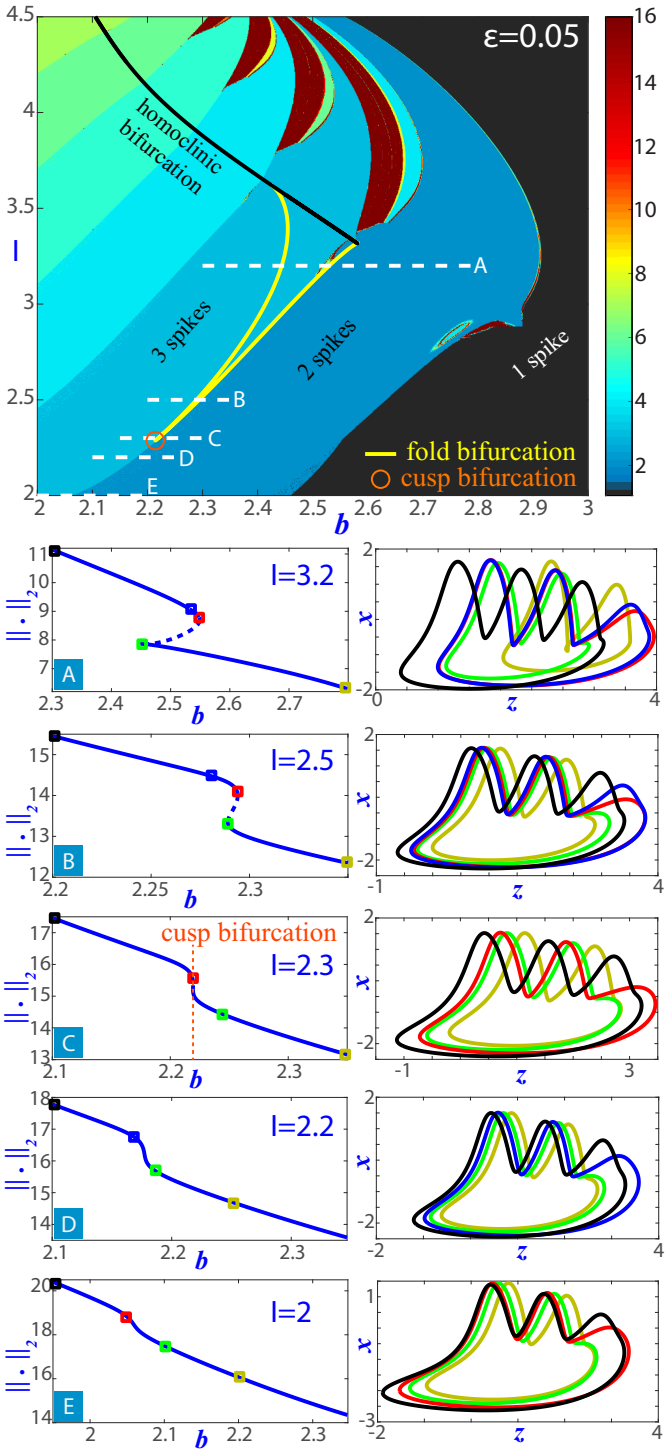

FIG. 9. Top: Biparametric bifurcation spike-counting diagram for $\varepsilon = 0.05$. Different segments are selected to illustrate the evolution from canard-induced continuous spike-adding (segments *A* and *B*) to Hopf-induced continuous spike-adding (segments *D* and *E*) through a cusp (segment *C*). Bottom: Left column shows bifurcation diagrams obtained by continuation corresponding to the selected segments. In the right column, some periodic orbits along the segment are plotted together to see their relative position and shape. The colors of the orbits correspond with coloured squares in the left bifurcation diagrams.

and 9.

As already mentioned, the transition from the region where spike-adding is induced by chaotic dynamics to the zones exhibiting continuous processes is determined, one way or another, by the homoclinic skeleton of the model. Two cases are clearly distinguished according to whether the dynamics change to either a canard-mediated mechanism or a Hopf-induced one.

If we pay attention to the transition towards a canard-induced spike-adding, the homoclinic bifurcation curve itself becomes a sharp frontier with the region governed by the chaotic machinery. Indeed, if we consider any horizontal line in the parameter space such that it crosses the homoclinic curve, as the long segment $R1$ in discontinuous orange in Fig. 2, the passage through the homoclinic curve is clearly the event which marks the change of behavior. As illustrated in Fig. 12, which is included in the Discussion section, the spike-adding transition from 2 to 3 spikes consists of a chaotic window (see Section II A), whereas in the passage from 3 to 4 spikes a bistability window is traversed (see Section II B). In between, the homoclinic curve is crossed, and large chaotic windows are no longer observed to the left of such bifurcation.

The transformation of discontinuous spike-addings into Hopf-induced ones is quite different. To describe how dynamics evolve, we have selected a short segment in the parameter space fixing $I = 4.1$ and $b \in [2.58, 2.6]$. We denote by $P1$ and $P2$ the left and right ends, respectively (see Fig. 2). The transition process starts when the segment crosses an ultimate fan of bifurcation curves of periodic orbits arising from the type-C inclination-flip (IF) codimension-two homoclinic bifurcation point located in the fold of the homoclinic curve (see the theoretical unfolding[34] and the numerically computed bifurcation curves displayed at the bottom-right panel in Fig. 10). As showed at top panels of Fig. 10, for $P1$ and $P2$ we observe a fold/Hopf and a fold/hom bursting, respectively. Some of the changes that occur in the attractor can be seen in the IBD bifurcation diagram (central panel of Fig. 10). By decreasing parameter b, a bistability zone is detected, which leads to the gaining of a new spike. It is formed as a consequence of the passing through fold and period-doubling bifurcation curves. Shortly after crossing this bistability zone, there is an abrupt change in the number of spikes that precedes the entrance into the domain of Hopf-induced spike-adding (see the green vertical band in the IBD). The time series and the orbit exhibited at the bottom-left panel in Fig. 10 show a phenomenon of intermittency where the fold/Hopf and the fold/Hom bursting alternate (the sum of the spikes of both types explains the abrupt jump observed in the IBD). We can understand this peculiar behavior appealing to the fast-slow decomposition. Along the transition from fold/Hopf to fold/hom bursting (see Fig. 1), the 2D fast manifold of limit cycles becomes tangent to the 1D slow manifold of equilibria. Close to this tangency, orbits can show the alternation between the two types of bursting, exhibiting phases where the orbit follows the fast manifold up to the Hopf bifurcation point and phases where orbits behave as if the fast manifold were split. The presence of the pencils of bifurcations that converge to the IF point helps in this mixed behavior.

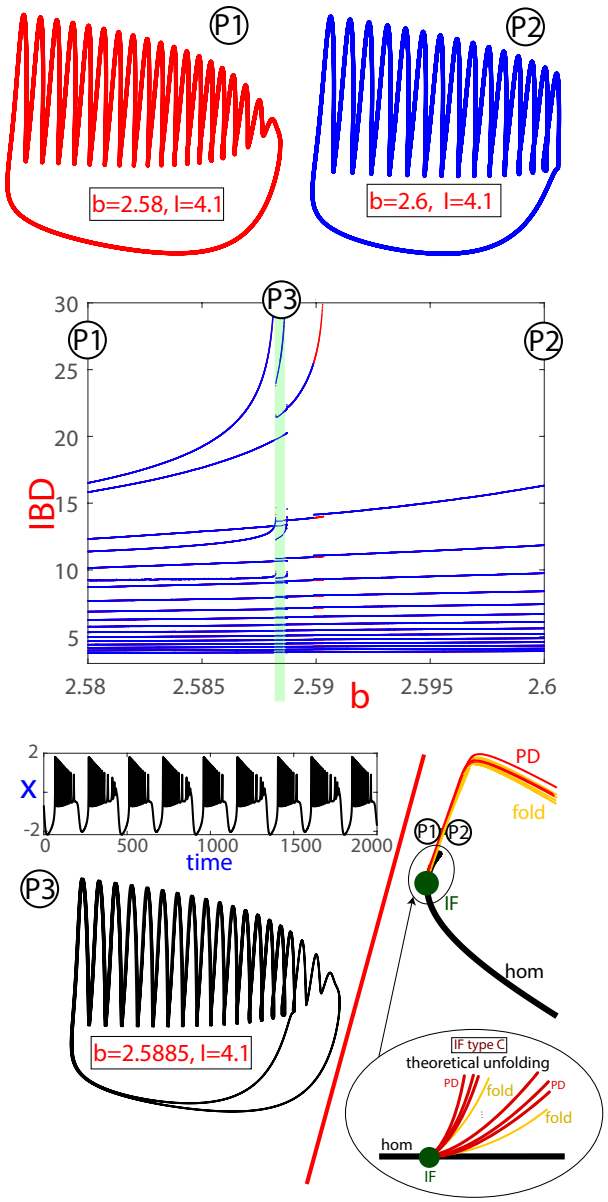

FIG. 10. Crossing the bridge between Hopf-induced (top-left) and chaos-induced (top-right) spike-adding. Orbits correspond to points P1 and P2, respectively, of Fig. 2. Inter-spike bifurcation diagram for $I = 4.1$ and $b \in [2.58, 2.6]$ is provided in central panel, where the green vertical band separates the two types of spike-adding. Transition through the green band is illustrated at the bottom-left panel. Bottom-right panel provides de location of P1 and P2, and also the numerically calculated bifurcation curves and the theoretical unfolding of a type-C inclination-flip.

IV. DISCUSSION

Throughout the previous sections we have provided a unified perspective of several of the spike-adding mechanisms that are unfolded in the Hindmarsh-Rose model and the transitions that occur between the different types. Figure 11 provides a schematic illustration of the catalogue. Specifically,

we have identified:

- **Chaos-induced spike-adding**: (translucent red region) discontinuous spike-adding formed by isolas of bursting periodic orbits with cascades of period-doubling bifurcations leading to chaos. This case corresponds to the chaotic scenario studied by Terman[23].

- **Canard-induced continuous spike-adding**: (translucent dark-blue region) continuous spike-adding created in hysteresis areas limited by fold bifurcations of periodic orbits and canards being involved in the genesis of extra spikes.

- **Hopf-induced continuous spike-adding**: (translucent pale-green region) continuous spike-adding with a Hopf bifurcation being involved in the creation of new extra spikes (see also Appendix).

- **Transition spike-adding states**: there are three possibilities. Translucent green strips shown in Fig. 11 correspond to the transition between Hopf-induced and canard-induced continuous spike-addings near a cusp bifurcation where two fold bifurcations of periodic orbits collapse. Sharp location is not possible because, as already explained in Section III, the cusp points are not easy to detect and, furthermore, they do not form a continuous line as they appear just at isolated points (they are codimension-two bifurcations). On the contrary, the frontier in between chaos-induced spike adding and the other two mechanisms is evident. The black curve (homoclinic bifurcation) marks the transition to canard-induced spike-adding. The change from chaos- to Hopf-induced spike-adding involves bifurcation curves of periodic orbits arising from codimension-two homoclinic bifurcations and it is clearly recognizable on the spike-counting bifurcation diagram.

Just as a summary of what is typically observed in numerical and experimental settings, Figure 12 shows a one parameter slice (line $R1$ in Fig. 2) where the three types of spike-adding detected in the model (chaos-induced discontinuous spike-adding (right), canard-induced continuous spike-adding (middle) and Hopf-induced continuous spike-adding (left)) and two transitions in between are observed. In the plot at the top (a), the interspike-interval bifurcation diagram (IBD) shows clearly the number of spikes and the time length among spikes. Red color represents coexistence of two periodic attractors with n and $n+1$ spikes. The bottom plot (b) presents the parametric evolution of the periodic orbits using continuation techniques. The figure shows the $\|\cdot\|_2$ norm of the periodic orbit along the selected segment $R1$. In the continuation line, the blue color line changes from Hopf-induced continuous spike-adding (left part) to canard-induced continuous spike-adding (middle part). Note that, on the right side, the purple color line represents an isola (simple closed curves in the corresponding slice) of 3-spikes periodic orbits and green and other colors represent the basic 2-spikes periodic orbit and its period-doubling bifurcated orbits on the region of

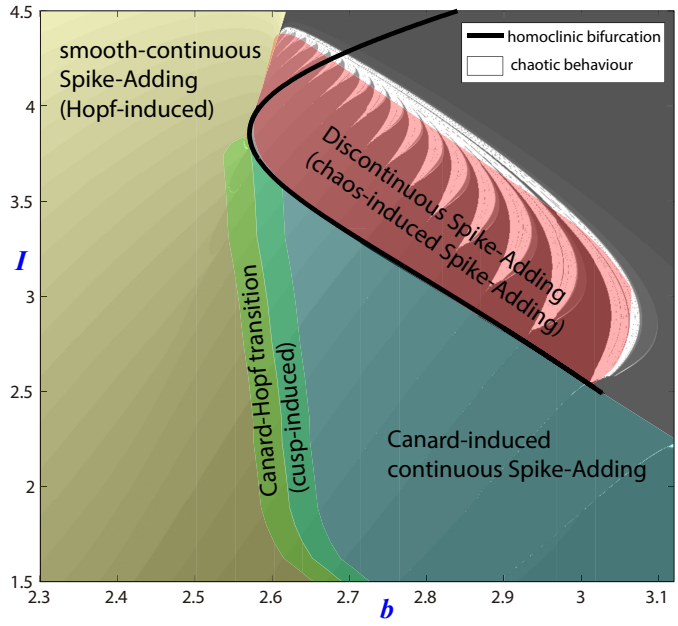

FIG. 11. Classification scheme of regions with different type of spike-adding process superimposed on the biparametric bifurcation spike-counting diagram for $\varepsilon = 0.01$. White color represents regions with chaotic behavior; different shades of gray represent regions with periodic orbits with different number of spikes; translucent colors represent (schematically) regions with different types of spike-adding. The homoclinic bifurcation (black curve) marks the boundary between the region with discontinuous spike-adding and the other regions.

chaos-induced discontinuous spike-adding. We can also observe how the change from the discontinuous spike-adding to the continuous spike-adding occurs sharply when crossing the homoclinic curve. On the other hand, while canard-induced continuous spike-adding is occurring, the segment $R1$ crosses bistability wedges, limited by a fold point and the first period-doubling bifurcation. When the last wedge has been crossed, the spike-adding mechanism changes to Hopf-induced. Note that bistability regions are only present in the canard-induced continuous spike-adding.

Fig. 12 also shows the vertical line ($b = 2.67434$) that, according to the fast-slow dynamics and the Izhikevich classification, corresponds to the passage from fold/hom to fold/Hopf bursting. Namely, in the biparametric plane (b,I), the vertical line $b = 2.67434$ is tangent to the homoclinic bifurcation curve for the fast subsystem at the point where the curve folds in the b-direction. Of course, since this useful classification is based on the limit case ($\varepsilon = 0$), this theoretical frontier works the better as smaller the value of ε is and, in fact, already for $\varepsilon = 0.01$ we observe how the Izhikevich criterion is no longer applicable in some regions.

Indeed, paying attention to the cascade of bifurcations shown at panel (b) of Fig. 12, it is still observed how on the left side of the vertical line of homoclinic folding, the canards are involved in the genesis of new spikes. On this side, the Izhikevich analysis classifies the bursting as fold/Hopf, but this only

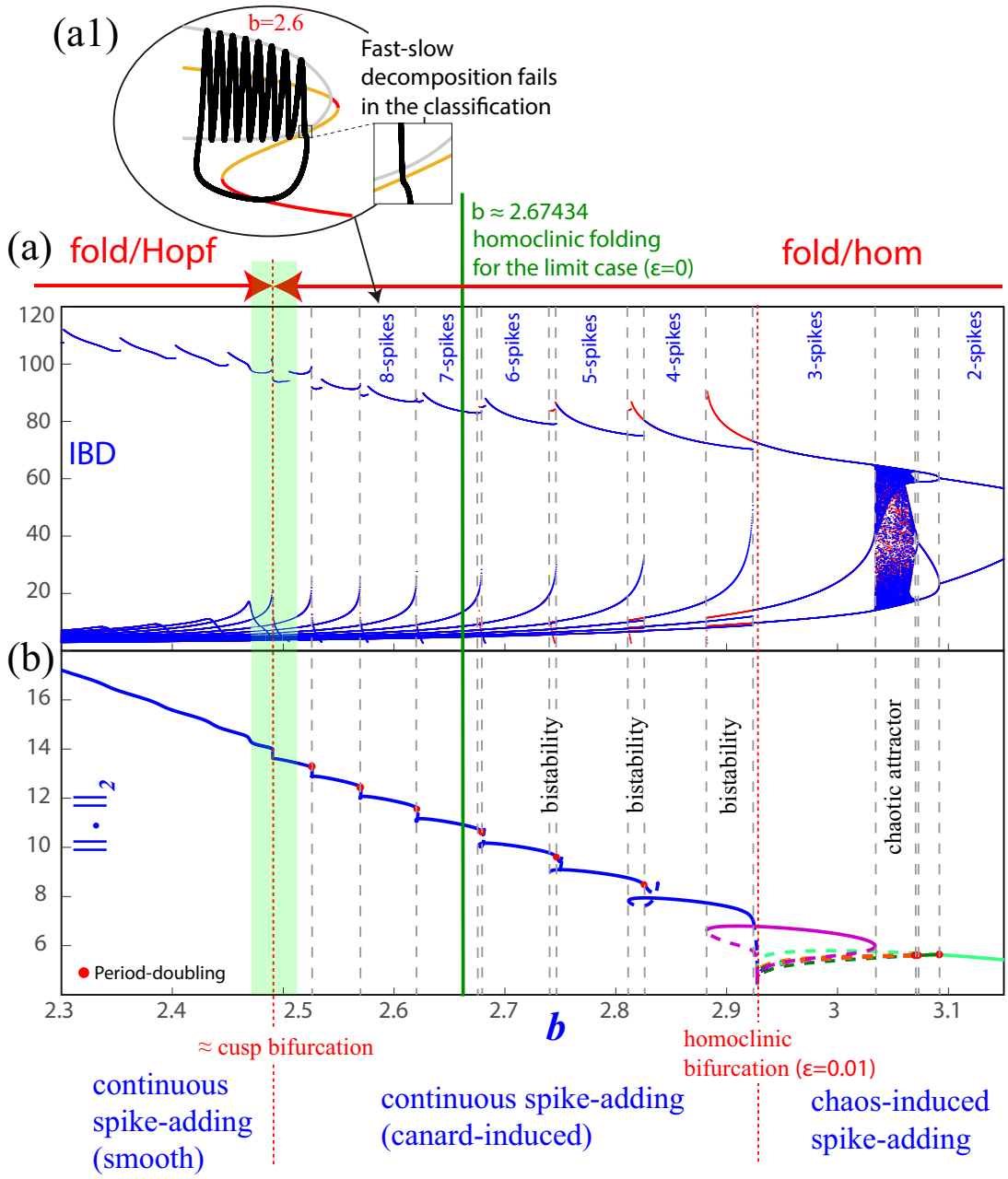

FIG. 12. Analysis of transitions along segment $R1$ (in Fig. 2) with $\varepsilon = 0.01$, $I = 2.75$ and b as bifurcation parameter. (a) Interspike-interval bifurcation diagram (IBD). Red color represents coexistence of two periodic attractors with n and $n+1$ spikes. Panel (b) shows the $\|\cdot\|_2$ norm of the periodic orbit along the process, obtained with continuation techniques (AUTO). Purple represents an isola of 3-spikes periodic orbits; the continuous spike-adding process is shown in blue; green and other colors represent the basic 2-spikes periodic orbit and its period-doubling bifurcated orbits. More details are given in the text. Panel (a1) illustrates one example of the limits with Izhikevich's classification.

manifests for smaller values of parameter b (on the left-side of the cusp bifurcation line, to be precise). The reason lies in the fact that for a higher dimensional parameter space, like in a three-dimensional bifurcation diagram including ε, the transition bifurcation surfaces exhibit some inclination, that is, they are not completely vertical (see recent Ref. 10 for a complete three dimensional analysis). Panel (a1) in Fig. 12 illustrates with an example the limitations with Izhikevich's classification. Superimposed on the fast-slow decomposition, a bursting orbit is shown. Fast-slow decomposition is fold/Hopf type, but bursting is clearly of fold/hom type.

From a practical point of view, we may have the following question: how does this study help in biological settings? In fact, the main point is to consider what phenomena we can expect. Obviously, it is not possible to determine the spike-adding mechanisms that a neuron experiences only with experimental data. Nevertheless, the visualization of a bursting orbit and the information obtained from biparametric maps

arising in simpler models can help us to point to one type or another. That is, if a square-wave bursting solution (fold/hom case) is observed, we should have in mind two possible spike-adding mechanisms: canard-induced or chaos-induced. If experimentation shows abrupt changes in the number of spikes, we can suspect that there is a hysteresis phenomenon and that the dynamics have been captured by an alternative stable branch, so we identify a canard-induced spike-adding. The recognition of this mechanism should move researcher to look for the coexisting stable orbit since bistability is, in many cases, a desirable feature of a neuron and may have biological consequences[35–37]. On the contrary, if some chaotic phenomenon is detected, we can suspect the existence of isolas and that the spike-adding processes may involve transitions through chaotic windows[38]. Furthermore, there are examples in the literature of experiments with neurons exhibiting comb-shaped biparametric structures associate to chaos-induced mechanisms[39–41]. In these examples, the use of biparametric maps helps to explain the results. The appearance of fold/Hopf bursting orbits is the signal that either bistability or chaos are over and the spike-adding becomes a smooth process. The above ones are not the only precursors of the different phenomena. For example, a bursting orbit that suddenly lengthens and then returns, but with an extra spike, can be identified with the presence of a canard phenomenon and bistability.

From a mathematical point of view, once the global structure is clear, one can think of obtaining analytical proofs to explain how the different processes and transformations emerge from the singular limit using, for instance, the techniques introduced by P. Carter[25,27]. We also remark that, taking into account that the codimension-two points are organizing centers for key bifurcations involved in some of the processes and transitions analysed in this paper, it should be interesting to study the existence of codimension-three points unfolding these codimension-two bifurcations, but we have to move into a three-parametric space, like in Ref. 10, and this is part of our future research.

V. CONCLUSIONS

Neural communication takes place through action potentials or spikes. In addition, it is when the spikes travel in packets that the exchange of information is more fluent and efficient. The number and tempo of the spikes in each burst are main ingredients to build neural messages. These are the reasons that justify the importance of the analysis of the spike-adding mechanisms. In this paper we deal with bursting in single-neurons activity. Among the most popular models, we choose the Hindmarsh-Rose, as it is the simplest one that is able to exhibit bursting behavior. We show and classify the different mechanisms of spike-adding: chaos-induced, canard-induced and Hopf-induced. Besides, we study the transition mechanisms from one type of spike-adding process to another.

The above processes involve bistable and chaotic regimes. As already mentioned, bistability is a profitable characteristic for a neuron and chaotic behaviors are commonly observed in experiments with real neurons in the laboratory, as in Refs. 38–41. Our theoretical results motivate the interest for discovering new mechanisms in the context of the cited experiments.

Spike-adding maps provide us with information on how we should move in the parameter space depending on whether we want our neuron to exhibit one or another spike-adding mechanism. These maps are common in the literature and similar chaotic zones and spike-adding stripes have been found for other realistic fold/hom bursting models, including the leech heart interneuron model[42] and the pancreatic β-cell neuron model[43], among others. Therefore, for future research, it would be interesting to explore whether this classification is valid in other models exhibiting fold/hom and fold/Hopf bursting, where we sincerely believe that this is the case. And what is more challenging, Izhikevich's catalogue for the types of bursting is extensive and one must wonder what spike-adding mechanisms are available in each case and also what are the transition dynamics.

ACKNOWLEDGMENTS

RB and SS have been supported by the Spanish Research projects PGC2018-096026-B-I00 and PID2019-105674RB-I00, the Universidad de Zaragoza-CUD project UZCUD2019-CIE-04 and the European Regional Development Fund and Diputación General de Aragón (E24-17R and LMP124-18). SI and LP have been supported by Spanish Research project MTM2017-87697-P. LP has been partially supported by the Gobierno de Asturias project PA-18-PF-BP17-072.

DATA AVAILABILITY

Data available on request from the authors. The simulations have been done using the AUTO[29,30] and TIDES[44,45] softwares.

[1] F. Zeldenrust, W. J. Wadman, and B. Englitz, Frontiers in Computational Neuroscience **12**, 48 (2018).
[2] R. Barrio and A. Shilnikov, Journal of Mathematical Neuroscience **1**, 6:1 (2011).
[3] J. G. Freire and J. A. C. Gallas, Phys. Chem. Chem. Phys. **13**, 12191 (2011).
[4] X.-B. Rao, Y.-D. Chu, Lu-Xu, Y.-X. Chang, and J.-G. Zhang, Communications in Nonlinear Science and Numerical Simulation **50**, 330 (2017).
[5] B. Jia, Chinese Physics B **23**, 030505 (2014).
[6] J. L. Hindmarsh and R. M. Rose, Proc. Roy. Soc. Lond. **B221**, 87 (1984).
[7] J. Rinzel, in *Mathematical Topics in Population Biology, Morphogenesis and Neurosciences: Proceedings of an International Symposium held in Kyoto, November 10–15, 1985*, edited by E. Teramoto and M. Yumaguti (Springer Berlin Heidelberg, Berlin, Heidelberg, 1987) pp. 267–281.
[8] E. M. Izhikevich, Int. J. Bifur. Chaos Appl. Sci. **10**, 1171 (2000).
[9] R. Barrio, S. Ibáñez, and L. Pérez, Phys. Lett. A **381**, 597 (2017).
[10] R. Barrio, S. Ibáñez, and L. Pérez, Chaos **30**, 053132, 20 (2020).
[11] R. Barrio, S. Ibáñez, L. Pérez, and S. Serrano, Commun. Nonlinear Sci. Numer. Simul. **83**, 105100, 15 (2020).
[12] R. Barrio, M. A. Martínez, S. Serrano, and A. Shilnikov, Chaos **24**, 023128 (2014).
[13] M. Desroches, T. J. Kaper, and M. Krupa, Chaos **23**, 046106 (2013).
[14] J. M. González-Miranda, Chaos **13**, 845 (2003).

[15] J. M. González-Miranda, Physical Review E **72**, 051922 (2005).
[16] J. M. Gonzalez-Miranda, Int. J. Bifur. Chaos Appl. Sci. **17**, 3071 (2007).
[17] G. Innocenti, A. Morelli, R. Genesio, and A. Torcini, Chaos **17**, 043128 (2007).
[18] G. Innocenti and R. Genesio, Chaos **19**, 023124 (2009).
[19] D. Linaro, A. Champneys, M. Desroches, and M. Storace, SIAM J. Appl. Dyn. Syst. **11(3)**, 939–962 (2012).
[20] M. Storace, D. Linaro, and E. de Lange, Chaos **18**, 033128 (2008).
[21] A. Shilnikov and M. Kolomiets, Int. J. Bifur. Chaos Appl. Sci. **18(8)**, 2141 (2008).
[22] N. Fenichel, J. Differential Equations **31**, 53 (1979).
[23] D. Terman, SIAM J. Appl. Math. **51**, 1418 (1991).
[24] J. Nowacki, H. M. Osinga, and K. Tsaneva-Atanasova, The Journal of Mathematical Neuroscience **2**, 7 (2012).
[25] P. Carter, Journal of Nonlinear Science **30**, 1432 (2020).
[26] C. Morris and H. Lecar, Biophys. J. **35**, 193 (1981).
[27] P. Carter and B. Sandstede, SIAM Journal on Applied Dynamical Systems **17**, 236 (2018).
[28] Y. A. Kuznetsov, *Elements of applied bifurcation theory*, 3rd ed., Applied Mathematical Sciences, Vol. 112 (Springer-Verlag, New York, 2004) pp. xxii+631.
[29] E. Doedel, in *Proceedings of the Tenth Manitoba Conference on Numerical Mathematics and Computing, Vol. I (Winnipeg, Man., 1980)*, Vol. 30 (1981) pp. 265–284.
[30] E. J. Doedel, R. Paffenroth, A. R. Champneys, T. F. Fairgrieve, Y. A. Kuznetsov, B. E. Oldeman, B. Sandstede, and X. J. Wang, `http://cmvl.cs.concordia.ca/auto`.
[31] Y. Pomeau and P. Manneville, Comm. Math. Phys. **74**, 189 (1980).
[32] E. Ott, *Chaos in dynamical systems*, 2nd ed. (Cambridge University Press, Cambridge, 2002) pp. xii+478.
[33] X. Wang, Physica D **62**, 263 (1993).
[34] A. J. Homburg and B. Sandstede, Handbook of Dynamical Systems **3**, 379 (2010).
[35] A. Dovzhenok and A. S. Kuznetsov, PLOS ONE **7**, 1 (2012).
[36] W. Barnett, G. O'Brien, and G. Cymbalyuk, Journal of Neuroscience Methods **220**, 179 (2013).
[37] M. Uzuntarla, Neurocomputing **367**, 328 (2019).
[38] H. Gu, Chaos **23**, 023126 (2013).
[39] W. Xiao-Bo, M. Juan, Y. Ming-Hao, Z. Qiao-Hua, G. Hua-Guang, and R. Wei, Chinese Physics Letters **25**, 2799 (2008).
[40] H. Gu, PLOS ONE **8**, 1 (2013).
[41] H. Gu, B. Pan, G. Chen, and L. Duan, Biological Cybernetics **78**, 391 (2014).
[42] R. Barrio, M. Lefranc, M. A. Martínez, and S. Serrano, EPL (Europhysics Letters) **109**, 20002 (2015).
[43] E. Mosekilde, B. Lading, S. Yanchuk, and Y. Maistrenko, BioSystems **63**, 3 (2001).
[44] A. Abad, R. Barrio, F. Blesa, and M. Rodríguez, `https://sourceforge.net/projects/tidesodes/`.
[45] A. Abad, R. Barrio, F. Blesa, and M. Rodríguez, ACM Transactions on Mathematical Software **39**, 5:1 (2012).

APPENDIX

In this Appendix we just show analytically, with a simple example, how an increase in the distance between the saddle-node bifurcations of equilibria in the fast subsystem of the HR model allows the increment of the number of spikes, and so, it generates the Hopf-induced spike-adding process.

Let us consider the following family of vector fields:

$$\begin{cases} x' &= -zx-\omega y-Lx(x^2+y^2), \\ y' &= \omega x-zy-Ly(x^2+y^2), \\ z' &= \varepsilon. \end{cases} \tag{A.1}$$

This is a toy-model for a Hopf bifurcation, where the bifurcation parameter z varies with respect to time at a constant ratio ε, which we assume to be a small parameter ($\varepsilon \ll 1$). Coefficient L corresponds to the first Lyapunov coefficient[28] and we assume that $L > 0$.

Using polar coordinates $x = r\cos\theta$, $y = r\sin\theta$ in (A.1), we get:

$$\begin{cases} r' &= -zr-Lr^3, \\ \theta' &= \omega, \\ z' &= \varepsilon. \end{cases} \tag{A.2}$$

Let

$$\varphi(t,r_0,\theta_0,z_0) = \\ \left(\varphi^r(t,r_0,\theta_0,z_0),\varphi^\theta(t,r_0,\theta_0,z_0),\varphi^z(t,r_0,\theta_0,z_0)\right)$$

be the flow defined by equations (A.2). Clearly,

$$\varphi^\theta(t,r_0,\theta_0,z_0) = \theta_0+\omega t, \\ \varphi^z(t,r_0,\theta_0,z_0) = z_0+\varepsilon t.$$

Fixing time $t = \frac{2\pi}{\omega}$ and angle $\theta_0 = 0$ we get the first return map P from the half-plane $\theta_0 = 0$ on itself. Namely,

$$P(r_0,z_0) = \left(P^r(r_0,z_0),P^z(r_0,z_0)\right)$$

with

$$P^r(r_0,z_0) = \varphi^r\left(\frac{2\pi}{\omega},r_0,0,z_0\right)$$

and

$$P^z(r_0,z_0) = \varphi^z\left(\frac{2\pi}{\omega},r_0,0,z_0\right) = z_0+\frac{2\pi\varepsilon}{\omega}.$$

In what follows, we assume that

$$(r_0,z_0) \in [0,R]\times\{-\delta\},$$

for some $\delta > 0$ and $R > \sqrt{\frac{\delta}{L}}$, and define

$$(r_n,z_n) = ((P^r)^n(r_0,z_0),(P^z)^n(r_0,z_0)).$$

Constant δ stands for the maximum allowed change in parameter z. We say that the orbit of the point $(r_0,0,z_0)$ has N spikes if N is the maximum number of iterations of the first return map which remain in the rectangle $[0,R]\times[-\delta,\delta]$. Since $R > \sqrt{\frac{\delta}{L}}$, it follows by construction that $r_n < R$ for all $n \in \mathbb{N}$. On the other hand

$$z_n = -\delta+\frac{2\pi\varepsilon\, n}{\omega},$$

and, in order to have $z_n > \delta$, the condition

$$n > \frac{\delta\omega}{\pi\varepsilon},$$

must be fulfilled. We obtain the expected results, that is, the number n of allowed spikes increases as either δ or the rotation speed ω increase. Bearing in mind the Hindmarsh-Rose model, the number of spikes in the fold/Hopf bursting increases as the distance (measured in the z-direction) between the two saddle-node bifurcation points in the fast subsystem (2δ in the toy model) increases.